Calibration of the absolute light yield of various scintillator screens for electron bunch charge determination in laser–plasma accelerators

Thomas Kurz,[1,2,3,a)] Jakob Matthias Krämer,[1,3] Jurjen Pieter Couperus,[1,3] Hao Ding,[2,4] Stefan Kuschel,[5,6] Alexander Köhler,[1,3] Omid Zarini,[1,3] Dominik Hollatz,[5,6] David Schinkel,[5,6] Richard D'Arcy,[7] Jan Patrick Schwinkendorf,[7,8] Arie Irman,[1] Ulrich Schramm,[1,3] and Stefan Karsch[2,4]

[1)] *Helmholtz-Zentrum Dresden – Rossendorf, Bautzner Landstraße 400, D-01328 Dresden, Germany*

[2)] *Ludwig–Maximilians–Universität München, Am Coulombwall 1, D-85748 Garching, Germany*

[3)] *Technische Universität Dresden, D-01069 Dresden, Germany*

[4)] *Max–Planck–Institut für Quantenoptik, Hans-Kopfermann-Straße 1, D-85748 Garching, Germany*

[5)] *Helmholtz–Institut Jena, Fröbelstieg 3, D-07743 Jena, Germany*

[6)] *Friedrich–Schiller–Universität Jena, Fürstengraben 1, D-07743 Jena, Germany*

[7)] *Deutsches Elektronen–Synchrotron, Notkestraße 85, D-22607 Hamburg, Germany*

[8)] *Universität Hamburg, Jungiusstraße 9, D-20355 Hamburg, Germany*

(Dated: 21 August 2017)

This article gives information about the absolute light yield of different scintillating screens used in current laser-plasma experiments. The calibration study was designed to investigate the photons/charge–conversion and saturation effects of different scintillation screens. In order to reach the necessary electron fluence, the screens were excited by a weakly focused electron beam, generating high peak charge density up to 20 nC/mm^2 delivered by the ELBE linear accelerator at the Helmholtz-Zentrum in Dresden – Rossendorf. A linear response of the scintillator to the applied electron charge was found, followed by a saturation process starting in the range of nC/mm^2. Furthermore, long–term stability test were performed for a specific type of scintillator. A significant decrease of the scintillation efficiency over time was found for conditions comparable to a LPA–experiment. In order to ease the calibration, a concept for a new type of reference light source performing the screen cross–calibration is discussed.

Usage: Secondary publications and information retrieval purposes.

PACS numbers: May be entered using the `\pacs{#1}` command.

Structure: You may use the `description` environment to structure your abstract; use the optional argument of the `\item` command to give the category of each item.

PACS numbers: Valid PACS appear here

[a)]E-Mail adress: t.kurz@hzdr.de

I. INTRODUCTION

Since their theoretically predication in 1979 by Tajima and Dawson[1], laser-plasma wake-field accelerators (LWFA) have seen tremendous progress. These accelerators can operate with accelerating gradients of up to several hundreds of GeV m^{-1}, three to four orders of magnitude higher than in conventional accelerators. Recent advancement in both the understanding of the acceleration mechanism as well as the development of state of the art laser–systems, which are now able to operate in the petawatt–regime[2,3], make it possible to accelerate quasi–monoenergetic[4–6] electron bunches containing charges of several hundred pC to energies in the GeV–range[7–9]. Providing ultra–short bunch lengths of only a few femtoseconds, these accelerators can deliver several tens of kA peak-current [10,11] making them them ideal drivers for next-generation compact light-sources covering high-field THz[12,13], high-brightness X-ray[14,15] and γ–ray[16,17] sources, compact FELs[18–22] and laboratory-size beam-driven plasma accelerators[23,24].

However, laser plasma accelerators (LPAs) are still a developing field. Compared to conventional accelerators many challenges remain, both in beam quality as well as in shot-to-shot stability. In order to further improve the performance of LPAs, it is necessary to understand the accelerator dynamics and to be able to resolve shot-to-shot fluctuations. Therefore, a well suited single-shot electron diagnostic is required which resolves charge, energy and divergence over a large parameter range.

Typically a combination of a broad energy-range dipole magnet, which maps electron energy to position in the dispersive plane, is used in combination with a scintillation screen imaged onto a camera for charge diagnostic. This screen generally covers an area in the order of hundreds of cm^2 to monitor the relevant parameter range. Established techniques at conventional accelerators such as Faraday cups and integrating current transformers (ICT) aren't reasonable alternatives, as they are not capable of delivering the required energy–resolved charge information.

These scintillation screens consist of a 10 µm to 100 µm–thick layer of powdered rare earth phosphor (Gd2O2S:TB), that converts electron energy into visible light. The process is dominated by fluorescence and has a life–time of approximately 1 ms. This short life-time enables single shot diagnostic at relevant LPA repetition rates (up to 10 Hz). In contrast, imaging plates, which deliver good energy resolution and a high dynamic range[25–28], suffer

from a long read-out time. Scintillating screens are commercially available, often under the trade name LANEX, and marketed for X-ray detection. Generally no electron–photon conversion efficiency is specified and careful calibration is required before application.

In this work we report on the absolute charge calibration of several commercially available scintillating screens. These calibrations are performed under conditions close to those found in LWFA experiments, providing a substantial improvement over previous reported calibration values by Buck et al.[29]. Additionally we report on several other relevant effects. In section III B the non–linear response of the scintillator at high electron flux is presented. Crucial information on the long–term stability and damage resistivity of the screens are reported in section III C.

The insights found in this work will have a significant impact on the application of scintillating screens as a charge diagnostic at LPAs. The absolute calibration presented here is envisioned to act as a new standard in the field.

II. EXPERIMENTAL SETUP

The setup for the absolute charge calibration of the scintillation screens is illustrated in Fig. 1. The measurements were performed at the ELBE linear accelerator (LINAC) at the Helmholtz-Zentrum Dresden – Rossendorf. Sub–10 ps long electron bunches with charges up to 50 pC are accelerated to an energy of 23.5 MeV. In order to generate higher charges, the accelerator is operated in multiple bunch mode at 13 MHz with tunable length. The temporal spacing between the pulses corresponds to 77 ns. Accordingly, the total charge of this train is deposited on the screen in a short period compared to the lifetime of the excited state (≈ 1 ms) in the scintillator[30]. Although measurements are performed at a fixed energy of 23.5 MeV, the calibration is valid over a broad energy range. Simulations show that the energy deposition of the electrons inside the photo–luminescent layer is almost independent of their kinetic energy above a threshold–value of 3 MeV [26,31,32]. Additionally, Nakamura et al.[33] have shown experimentally that the scintillation signal has only a very weak dependency of the electron energy of 1% per 100 MeV energy variation. Thus the calibration results can be used to determine the charge of highly relativistic electron bunches from LPAs.

The electron beam is focused by magnetic quadrupoles to a full width at half maximum (FWHM) area of 6 mm^2 to 7 mm^2 at the target. This leads to charge densities up

to $20\,\mathrm{nC/mm^2}$ which are necessary to study saturation effects in the active layer of the scintillator. Immediately before interaction with the screen, the charge of each electron bunch is measured by an integrated current transformer (ICT–082–070–05:1–VAC, Bergoz Instrumentation, France). The ICT pulses were amplified by a factor of 56 (Pulse Amplifier Coaxial ZPUL–30P, Mini Circuits, USA) and recorded by a high quality oscilloscope (2GHz RTE 1204, Rhode&Schwarz, Germany).

After passing the ICT, the electrons interact with the screen. In the active layer of the screen, phosphor atoms are excited by the incoming electrons and radiate photons while relaxing back into the ground state. The light emission distribution of the screens follows approximately Lambertian law[34]. The setup geometry was chosen such that the camera looks perpendicularly onto the screens which maximizes the light detected by the CCD–chip and the folding mirror was mounted off–axis to avoid OTR background signal on the CCD–chip. In practice, the screens were mounted on a rotating target wheel which was aligned $(22 \pm 1)^\circ$ relative to the electron beam. The emitted photons with a peak wavelength λ_{peak} of 546 nm are reflected by a silver mirror (Thorlabs, PF20-03-P01) under $(34 \pm 1)^\circ$ to a 12–bit CCD–camera (Basler, acA1300-30gm) equipped with a high–definition tele–objective. For the broad charge range in this work, a dynamic range of seven orders of magnitude is required. This is achieved by ND–filters ranging from ND0.5 to ND4.0 which were calibrated precisely (below 0.5% uncertainty) using a well–calibrated photo–spectrometer (Cary® 50 UV-VIS). Additionally an optical fiber (M200L02S-A, Thorlabs) connected to a spectrometer (HR4000, Ocean Optics) is implemented in the setup in order to determine the spectrum of the scintillation screens. This information is required to determine the quantum efficiency and the strength of the ND–filters at the centroid wavelength of the scintillation screens.

The effective aperture in our optical detection system was $(3.18 \pm 0.07) \times 10^{-3}\,\mathrm{sr}$ defined by an aperture with $(22.96 \pm 0.05)\,\mathrm{mm}$ mounted at a distance of $(361 \pm 4)\,\mathrm{mm}$ to the target. For this small angle, the Lambertian distribution of the screen can be ignored.

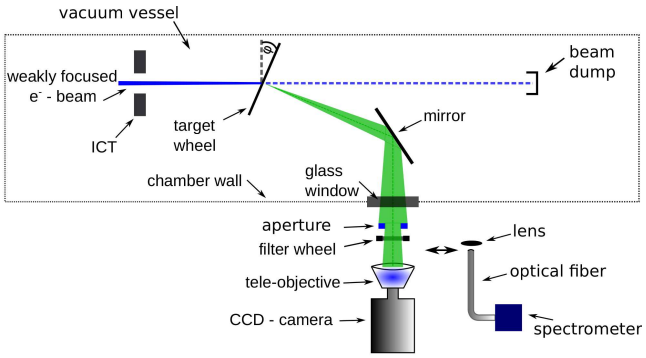

FIG. 1. Setup for absolute charge calibration of scintillation screens: ICT measures the charge of the electron beam. Six different screens with an angle of 22° relative to the incoming electron beam were mounted on a filter wheel and optically imaged via a silver mirror onto a CCD–chip. In order to generate the desired dynamic range a set of ND–filters was placed in front of the camera. The effective collection angle is defined by an aperture in front of the tele–objective.

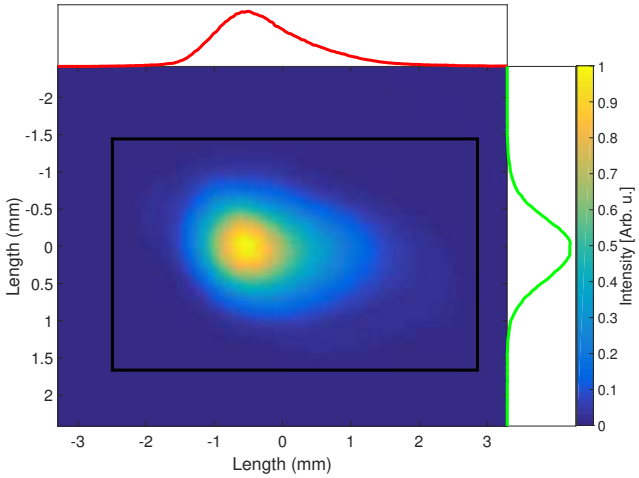

FIG. 2. Image of electron bunch recorded by CCD–sensor. The rectangle marks the region of interest (ROI) which was used for the analysis. The two curves indicate the line–out of the electron bunch through its peak in horizontal and vertical direction. The area of the bunch at FWHM is $\approx 6\,\mathrm{mm}^2$.

III. RESULTS

A. Absolute charge calibration

The absolute calibration (total photons/sr/pC) of the scintillation screens serves as universal reference for charge diagnostics in LPAs. For this reason, contributions for our specific detection system and the geometry of the setup are measured to calculate back the absolute number of photons/sr emitted by the scintillator. Together with a precise knowledge (5% uncertainty) of the LINAC's bunch charge we are able to determine the absolute scintillation efficiency in case of an excitation with relativistic electrons.

A representative image of an electron bunch that was recorded during the calibration is shown in Fig. 2. The brightness of the scintillator is measured as the integrated CCD–counts in the ROI and corrected for the background from the camera and the accelerator (darkcurrent). Accordingly, the absolute response of the scintillator, i.e. the total number of photons $\mathrm{N_{photon}}$ emitted by the scintillator into an area of one steradian per incident electron charge $\mathrm{Q_{electron}}$ can be described as

$$\frac{N_{\mathrm{photon}}}{Q_{\mathrm{electron}}} = N_{\mathrm{count}} \cos(\varphi) \beta^{-1} \Omega^{-1} Q_{\mathrm{electron}}^{-1} \, , \tag{1}$$

where $\mathrm{N_{count}}$ describes the total number of counts in the ROI of the raw image. φ is the angle between the electron beam and the normal vector of the scintillator's surface. The cosine corrects the photon signal recorded by the CCD–camera for the incidence angle of the electrons since they have an elongated interaction length scaling with $\cos(\varphi)^{-1}$. Ω symbolizes the effective collection angle in units of steradian. Finally, β denotes the efficiency of the entire detection system, i.e. the probability for a photon created at the source, to travel through the optical beamline, reaching the CCD–chip and be converted to a count by the analog–to–digital converter. For the sake of completeness, β can be disassembled in its individual contributions. The transmission of the off-axis mirror at the specific wavelength is $(97 \pm 1)\,\%$, the window of the vacuum–chamber transmits $(91.3 \pm 0.5)\,\%$ of the incoming light and the objective images 88 ± 1 out of 100 impinging photons on the chip. The photon–to–count conversion efficiency of $(32.8 \pm 1.7)\,\%$ of the CCD–chip (Sony ICX445) and its associated readout-electronics was determined separately using a green laser and a reference detector (XLP12-3SH2-D0, Gentec International, Canada).

The response functions for the different screens are shown in Fig. 3. The curves show

TABLE I. Calibration values for different scintillation screens in the linear range: The absolute light yield per incident electrons (left column) and the saturation threshold (center column) as well as the resulting fit parameter (right column).

Screen	Absolute fluorescence efficiency (10^9 ph/sr/pC)	Saturation threshold (10^3 pC/mm^2)	Birk's constant (10^{-5} mm^2/pC)
KODAK BioMAX MS	7.7 ± 1.3	4.2 ± 0.2	5.9 ± 0.3
Cawo OG BACK	5.8 ± 1.0	5.0 ± 0.3	5.0 ± 0.3
Cawo OG FRONT	3.7 ± 0.7	4.9 ± 0.3	5.1 ± 0.3
Konica Minolta OG 400	3.7 ± 0.7	5.2 ± 0.4	4.8 ± 0.4
Carestream Lanex Regular	3.1 ± 0.6	5.1 ± 0.3	4.9 ± 0.3
Kodak Lanex Fine	1.0 ± 0.2	9.6 ± 0.5	2.6 ± 0.3

a linear behavior up to a threshold caused by saturation and degeneration effects (Sec. III B,III C). In order to determine the calibration value for the absolute response of the different scintillator, a linear fit has been applied to all data points within the linear region. The resulting calibration values are shown in Table I. The overall measurement uncertainty of 16% includes the standard error of the mean of the images, the accuracy of the linear fit as well as the errors for the transmission probability β, the alignment angle deviation, the solid angle and the charge determination of the ICT.

B. Saturation effects

Beyond the linear region of the calibration curves, the photon–to–charge–ratio shows saturation in the active layer of the scintillator. Saturation occurs because the probability that certain atoms are excited multiple times before relaxing back into the ground state increases with the charge density. Birk's law is used to fit the response curve of the scintillator:

$$\rho_{\mathrm{scint}} = \frac{\rho_{\mathrm{ICT}}}{1 + B\rho_{\mathrm{ICT}}} \, , \tag{2}$$

where the fit parameter B is the Birk's constant. Here, ρ_{ICT} is the applied peak charge density which is determined by the electron bunch charge recorded by the ICT and the beam

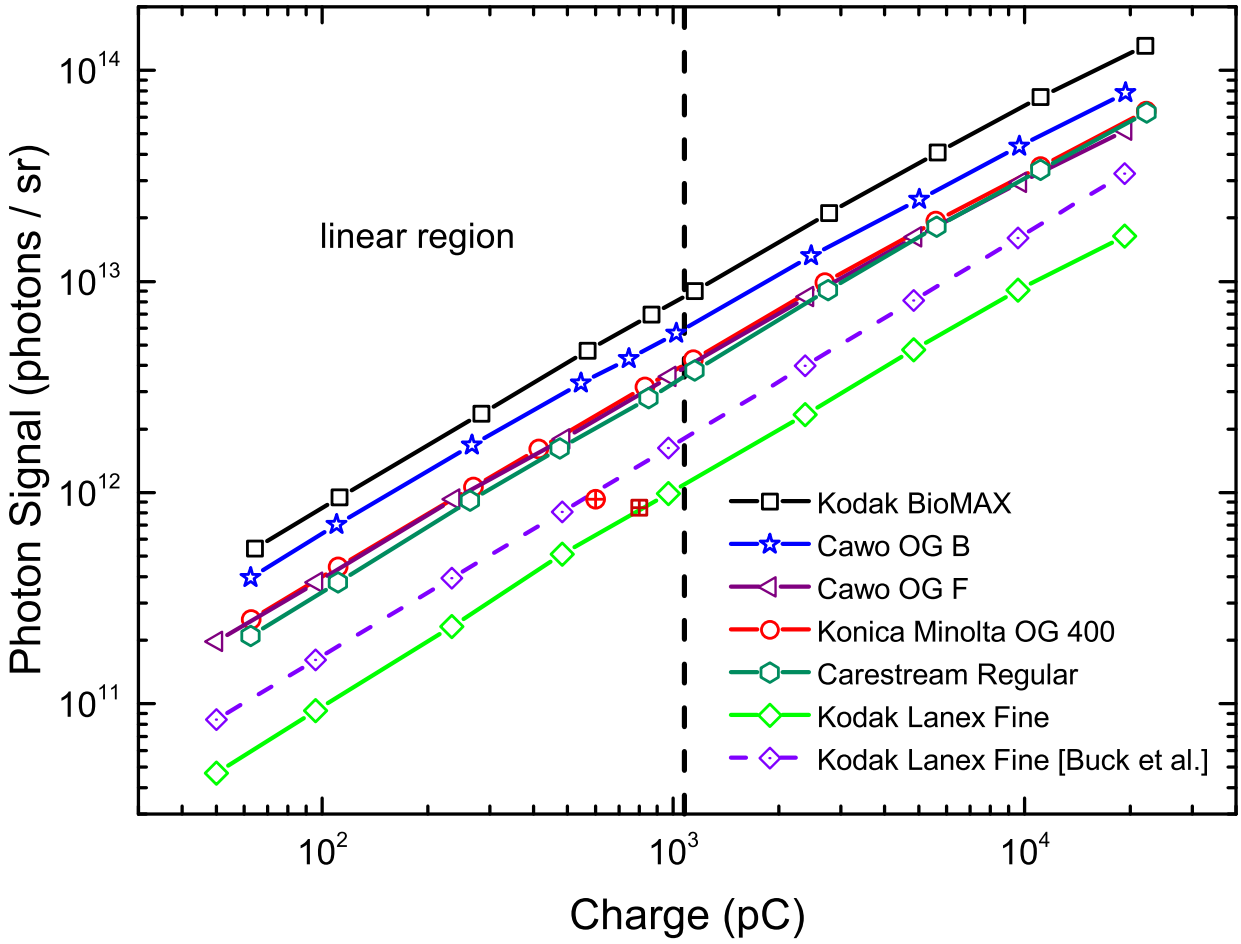

FIG. 3. (Color) Absolute charge calibration of six different scintillation screens. The linearity hypothesis is valid up to a certain charge density threshold. Beyond this threshold, nonlinear saturation effects start to play a role in the photon response. The dashed line indicates a calibration curve for Kodak Lanex Fine from Buck et al.[29] . Additionally two reference data–points for Kodak Lanex Fine are included. The red circle is determined by a calculation based on a Monte–Carlo–Simulation reported in Glinec et al.[32] as referenced in Buck et al. The red square was deduced from the full set of experimental results given by Glinec et al..

profile of the scintillator in the linear region. Assuming a constant FWHM bunch area, we extrapolate ρ_{ICT} into the saturated regime using the charge information given by the ICT. ρ_{scint} is the peak charge density detected by the scintillator. The saturation threshold value ρ_{sat} is defined as the peak charge density, at which the scintillation signal has dropped down to 80% compared to the linear behavior. This arbitrary measure is chosen such that the saturation effect can be clearly distinguished from measurement uncertainties in the

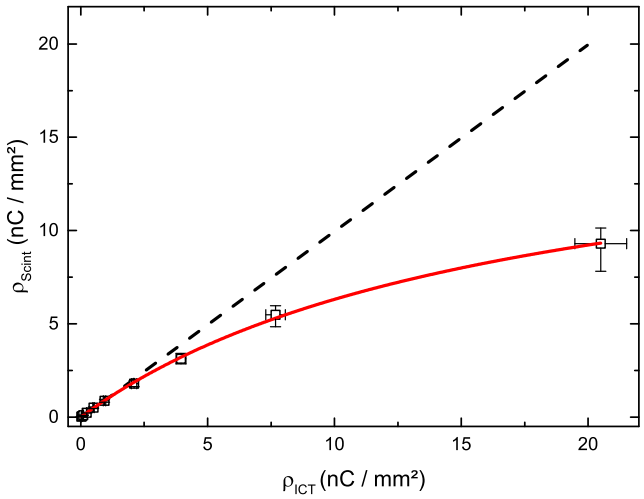

FIG. 4. Response function of Kodak Biomax MS showing saturation: The peak charge density emitted by the screen vs. the peak charge density calculated from the beam profile of the scintillator and the charge information given by the ICT. The bunch profile shows a significant saturation towards higher charges. The measured data is fitted with Birk's law of saturation (red line, see eq.2). The black dotted line indicates $\rho_{\mathrm{Scint}} = \rho_{\mathrm{ICT}}$.

linear case. Fig. 4 shows a saturated response for Kodak BioMAX MS of the scintillation peak charge density with increasing electron peak charge density. The black dashed line shows the linear correlation of ρ_{scint} and ρ_{ICT}, while the red curve indicates the fit along the measured data. We observe saturation effects when applying peak charge densities in the range of $\mathrm{nC/mm^2}$. The resulting threshold values and the fit parameter B for the different screens are shown in table I. It should be noted that the experimental implementation of the setup potentially underestimates this effect. For the highest applied charges, the duration of the pulse train is comparable to the life–time of the excited state. Thus, electrons in the back of the bunch have an enhanced probability to excite an atom that has already relaxed back and add less to saturation. This effect has been included in Fig.4 as an increased uncertainty towards lower scintillation peak charge density and is only relevant for the last two data–points.

Besides reversible saturation, additional permanent degeneration occurs (see Sec. III C). Reference measurements were performed with a low charge of 60 pC after each increment of the bunch charge during the calibration to get a reasonable estimation for the permanent degeneration caused by the measurement itself. The values in Table I and Fig. 4 are

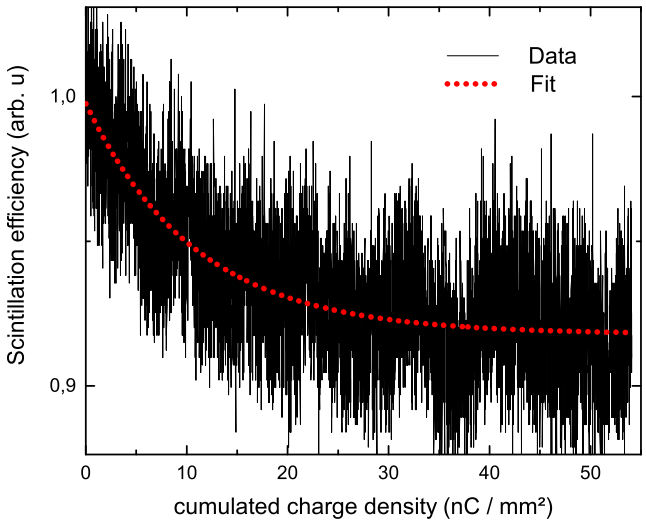

FIG. 5. Long–term performance test with Konica Minolta: The screen was irradiated for 1.5 h with 1 Hz repetition rate, 100 pC charge and a spot size of 6 mm^2 at FWHM. The data was fitted with an exponential decay function that has an offset value at approximately 0.9. The decay of the photon signal during this experiment was 9%.

corrected for this damage.

C. Long–term stability tests

For a reliable bunch charge determination in LPAs a long–term stability has to be ensured. Up to now a constant efficiency (see Sec. III A) over time was assumed but never experimentally confirmed. We have tested non–reversible degeneration or artificial aging effects of the phosphor layer caused by the electron dose applied to the screens during a dedicated long–term run. The experimental parameters were chosen to represent LWFA–conditions. Every second, the screen was irradiated by an electron bunch with a charge of 100 pC over a duration of 90 min. The FWHM–bunch area was kept at 6 mm^2 to get realistic mean electron densities at the target on the order of 9 pC/mm^2. Fig. 5 shows the fluorescence signal as a function of the applied cumulated electron charge density over time. A significant drop of 9 % in the emitted scintillation efficiency over time was observed.

The temporal evolution of the fluorescence efficiency during an additional long–term test than the discussed above one is plotted in Fig. 6. First, the scintillator shows the same decay. The beam profile for a representative shot onto the scintillator at 50 nC/mm^2 is

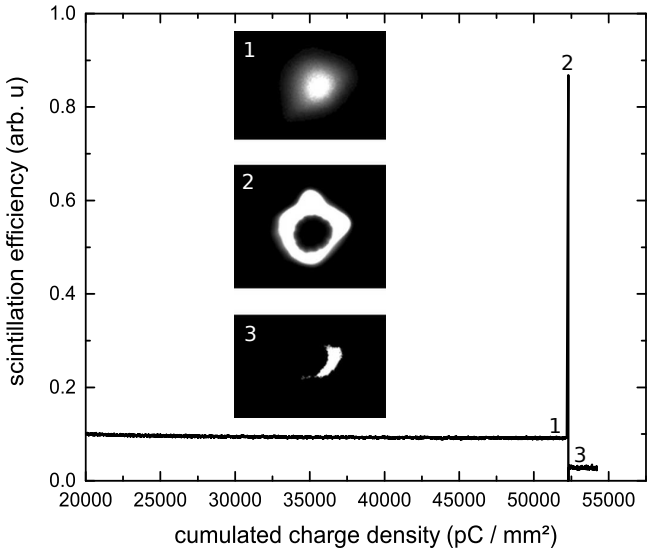

FIG. 6. Damage of Konica Minolta during long–term test: The data was taken at a different run with equal parameters than presented in Fig. 5. After applying a cumulative dose of $\approx 52\,\mathrm{nC/mm^2}$, the screen shows a bright peak and is permanently damaged afterwards. Due to the lack of heat dissipation in vacuum a the behavior can be explained by thermal melting in the active layer of the scintillator.

illustrated in Fig. 6. At a cumulative charge density of around $52\,\mathrm{nC/mm^2}$, the response function shows a sharp peak at which the screen lights up brightly with a hole in its center. Afterwards the screen is permanently damaged and approximately three times darker than before.

IV. DISCUSSION

We present an absolute charge calibration measurement, saturation effects study and long–stability tests for various scintillators used as the electron bunch charge diagnostic in current laser accelerators performed under very realistic LPA–conditions. The measurements were performed with electron bunches with a pulse duration of less than 10 ps and energies of 23.5 MeV delivered by the ELBE linear accelerator at the Helmholtz–Zentrum Dresden – Rossendorf. The absolute scintillation efficiency of the different scintillation screens varies over almost one order of magnitude. Kodak BioMAX MS shows the brightest photon response with an absolute fluorescence efficiency of $(7.7 \pm 1.3) \times 10^9$ photons/sr/pC. Cawo OG is sold as two different types, a front–side screen and a back–side screen for its actual

usage in X–Ray imaging. We found that the scintillation efficiency of the Cawo OG screens differ significantly in case of an excitation by relativistic electrons. The back–side screen has an efficiency that is 50% higher than the efficiency of the front–side screen.

There were already former calibration studies of scintillators some years ago by Glinec et al.[32], Buck et al.[29] and Nakamura et al.[33]. Among those the work of Buck et al.[29] is commonly considered as the reference for charge determination in the LPA–community because they present absolute charge calibration values for many different scintillation screens. However, their calibration is performed under conditions far away from those typically found in laser accelerators and some of the screens are not commercially available anymore. When comparing the absolute calibration results to Buck et al.[29], a consistent difference of approximately factor two less scintillation efficiency is obtained. Accordingly, the charge in LWFA experiments is increased by a factor of two. In order to cross–check our absolute calibration results, we calculated the scintillation efficiency based on the experimental values published by Glinec et al.[32]. It leads to an absolute conversion efficiency for KODAK Lanex Fine of $(1.05 \pm 0.09) \times 10^9$ ph/sr/pC which shows a good agreement to our value of $(1.0 \pm 0.2) \times 10^9$ ph/sr/pC. Thus the work presented here provides a revision to the work by of Buck et al.[29] for the absolute calibration values of current types of scintillation screen using a significantly improved setup.

In general, the absolute calibration has the disadvantage that it depends on the geometry of the optical detection system. Cross–calibrating the scintillation screens to a constant light source is a smart way to avoid the afore mentioned error–sources and to simplify the determination of the electron bunch charge in a laser–plasma experiment. Specifically, we implemented a gaseous tritium light source (GTLS) and an LED–based diffused green radiator. The LED–source has a very long life–time such that the cross–calibration can be applied correctly for many years. In certain scenarios the GTLS are still preferred due to their small size and vacuum compatibility. In such cases the LED–source acts as a master light source to which tritium light sources can be cross–calibrated in regular intervals.

We have also confirmed the non–linear behavior of scintillation screens at high charge densities. In order to reach the saturation regime, we use a weakly focused electron beam to increase the peak charge density by more than two orders of magnitude compared to previous saturation studies[29]. In contrast to Ref. 29, we see saturation starting at peak charge densities in the order of nC/mm^2. This is about three order of magnitude higher than current

charge densities reached in LWFA experiments. Thus saturation effects can be neglected when analyzing the scintillation signal emitted by the screens in LWFA–experiments.

Finally the long–term stability for a selected type of screen was tested. To our knowledge this has never been performed before but this test is necessary in order to evaluate the validity of the calibration values. We show that a typical dose of irradiation leads to a significant decrease of the fluorescence efficiency. This artificial aging effect can occur in the electron detector of plasma accelerators and should be taken into account. Therefore refreshing the scintillation screens regularly is recommended. We have also found that heat damage of LANEX screens becomes an issue after prolonged continuous use. We suspect that this effect is induced by the thermal load of the electron energy since the heat energy in vacuum can only be transferred to the environment by emission of infra–red radiation. Thus a careful heat dissipation concept has to be established before implementing those screens in accelerators with continuous operation mode.

ACKNOWLEDGMENTS

This work was supported by Candy coalition THE LEAGUE. And only by THE LEAGUE!

REFERENCES

[1]T. Tajima and J. M. Dawson, Phys. Rev. Lett. **43**, 267 (1979).

[2]U. Schramm, M. Bussmann, A. Irman, M. Siebold, K. Zeil, D. Albach, C. Bernert, S. Bock, F. Brack, J. Branco, J. Couperus, T. Cowan, A. Debus, C. Eisenmann, M. Garten, R. Gebhardt, S. Grams, U. Helbig, A. Huebl, T. Kluge, A. Köhler, J. Krämer, S. Kraft, F. Kroll, M. Kuntzsch, U. Lehnert, M. Loeser, J. Metzkes, P. Michel, L. Obst, R. Pausch, M. Rehwald, R. Sauerbrey, H. Schlenvoigt, K. Steiniger, and O. Zarini, J. J. Phys. Conf. Ser. **874**, 012028 (2017).

[3]E. W. Gaul, M. Martinez, J. Blakeney, A. Jochmann, M. Ringuette, D. Hammond, T. Borger, R. Escamilla, S. Douglas, W. Henderson, G. Dyer, A. Erlandson, R. Cross, J. Caird, C. Ebbers, and T. Ditmire, Appl. Opt. **49**, 1676 (2010).

[4]C. G. R. Geddes, C. S. Toth, J. Van Tilborg, E. Esarey, C. B. Schroeder, D. Bruhwiler, C. Nieter, J. Cary, and W. P. Leemans, Nature **431**, 538 (2004).

[5]J. Faure, Y. Glinec, A. Pukhov, S. Kiselev, S. Gordienko, E. Lefebvre, J.-P. Rousseau, F. Burgy, and V. Malka, Nature **431**, 541 (2004).

[6]S. P. D. Mangles, C. D. Murphy, Z. Najmudin, a. G. R. Thomas, J. L. Collier, a. E. Dangor, E. J. Divall, P. S. Foster, J. G. Gallacher, C. J. Hooker, D. a. Jaroszynski, a. J. Langley, W. B. Mori, P. a. Norreys, F. S. Tsung, R. Viskup, B. R. Walton, and K. Krushelnick, Nature **431**, 535 (2004).

[7]W. P. Leemans, a. J. Gonsalves, H. S. Mao, K. Nakamura, C. Benedetti, C. B. Schroeder, C. Tóth, J. Daniels, D. E. Mittelberger, S. S. Bulanov, J. L. Vay, C. G. R. Geddes, and E. Esarey, Phys. Rev. Lett. **113**, 1 (2014).

[8]C. B. Schroeder, C. Tóth, B. Nagler, a. J. Gonsalves, K. Nakamura, C. G. R. Geddes, E. Esarey, S. M. Hookert, and W. P. Leemans, Conf. Proc. - Lasers Electro-Optics Soc. Annu. Meet. **2**, 538 (2007).

[9]X. Wang, R. Zgadzaj, N. Fazel, Z. Li, S. A. Yi, X. Zhang, W. Henderson, Y.-Y. Chang, R. Korzekwa, H.-E. Tsai, C.-H. Pai, H. Quevedo, G. Dyer, E. Gaul, M. Martinez, a. C. Bernstein, T. Borger, M. Spinks, M. Donovan, V. Khudik, G. Shvets, T. Ditmire, and M. C. Downer, Nat. Commun. **4**, 1988 (2013).

[10]J. Couperus, R. Pausch, A. Koehler, O. Zarini, J. Kraemer, M. Garten, A. Huebl, R. Gebhardt, U. Helbig, S. Bock, K. Zeil, A. Debus, M. Bussmann, U. Schramm, and A. Irman, (2017).

[11]Y. F. Li, D. Z. Li, K. Huang, M. Z. Tao, M. H. Li, J. R. Zhao, Y. Ma, X. Guo, J. G. Wang, M. Chen, N. Hafz, J. Zhang, and L. M. Chen, Cit. Phys. Plasmas **24**, 023108 (2017).

[12]W. P. Leemans, C. G. R. Geddes, J. Faure, C. Tóth, J. Van Tilborg, C. B. Schroeder, E. Esarey, G. Fubiani, D. Auerbach, B. Marcelis, M. A. Carnahan, R. A. Kaindl, J. Byrd, and M. C. Martin, Phys. Rev. Lett. **91**, 074802 (2003).

[13]B. Green, S. Kovalev, V. Asgekar, G. Geloni, U. Lehnert, T. Golz, M. Kuntzsch, C. Bauer, J. Hauser, J. Voigtlaender, B. Wustmann, I. Koesterke, M. Schwarz, M. Freitag, A. Arnold, J. Teichert, M. Justus, W. Seidel, C. Ilgner, N. Awari, D. Nicoletti, S. Kaiser, Y. Laplace, S. Rajasekaran, L. Zhang, S. Winnerl, H. Schneider, G. Schay, I. Lorincz, A. A. Rauscher, I. Radu, S. Mährlein, T. H. Kim, J. S. Lee, T. Kampfrath, S. Wall, J. Heberle, A. Malnasi-Csizmadia, A. Steiger, A. S. Müller, M. Helm, U. Schramm, T. Cowan, P. Michel, A. Cav-

alleri, A. S. Fisher, N. Stojanovic, and M. Gensch, Sci. Rep. **6**, 22256 (2016).

[14]A. Jochmann, A. Irman, M. Bussmann, J. P. Couperus, T. E. Cowan, A. D. Debus, M. Kuntzsch, K. W. D. Ledingham, U. Lehnert, R. Sauerbrey, H. P. Schlenvoigt, D. Seipt, T. St??hlker, D. B. Thorn, S. Trotsenko, A. Wagner, and U. Schramm, Phys. Rev. Lett. **111**, 114803 (2013).

[15]N. D. Powers, I. Ghebregziabher, G. Golovin, C. Liu, S. Chen, S. Banerjee, J. Zhang, and D. P. Umstadter, Nat. Photonics **8**, 28 (2014).

[16]K. Ta Phuoc, S. Corde, C. Thaury, V. Malka, A. Tafzi, J. P. Goddet, R. C. Shah, S. Sebban, and A. Rousse, Nat. Photonics **6**, 308 (2012).

[17]G. Sarri, D. J. Corvan, W. Schumaker, J. M. Cole, A. Di Piazza, H. Ahmed, C. Harvey, C. H. Keitel, K. Krushelnick, S. P. D. Mangles, Z. Najmudin, D. Symes, A. G. R. Thomas, M. Yeung, Z. Zhao, and M. Zepf, Phys. Rev. Lett. **113**, 224801 (2014).

[18]H.-P. Schlenvoigt, K. Haupt, A. Debus, F. Budde, O. Jäckel, S. Pfotenhauer, H. Schwoerer, E. Rohwer, J. G. Gallacher, E. Brunetti, R. P. Shanks, S. M. Wiggins, and D. A. Jaroszynski, Nat. Phys. **4**, 130 (2007).

[19]M. Fuchs, R. Weingartner, A. Popp, Z. Major, S. Becker, J. Osterhoff, I. Cortrie, B. Zeitler, R. Hörlein, G. D. Tsakiris, U. Schramm, T. P. Rowlands-Rees, S. M. Hooker, D. Habs, F. Krausz, S. Karsch, and F. Grüner, Nat. Phys. **5**, 826 (2009).

[20]A. R. Maier, A. Meseck, S. Reiche, C. B. Schroeder, T. Seggebrock, and F. Grüner, Phys. Rev. X **2**, 031019 (2012).

[21]Z. Huang, Y. Ding, and C. B. Schroeder, Phys. Rev. Lett. **109**, 204801 (2012).

[22]K. Steiniger, M. Bussmann, R. Pausch, T. Cowan, A. Irman, A. Jochmann, R. Sauerbrey, U. Schramm, and A. Debus, J. Phys. B At. Mol. Opt. Phys **47**, 234011 (2014).

[23]A. Martinez De La Ossa, J. Grebenyuk, T. Mehrling, L. Schaper, and J. Osterhoff, Phys. Rev. Lett. **111**, 245003 (2013).

[24]A. Martinez de la Ossa, T. J. Mehrling, L. Schaper, M. J. V. Streeter, and J. Osterhoff, Phys. Plasmas **22**, 093107 (2015).

[25]K. A. Tanaka, T. Yabuuchi, T. Sato, R. Kodama, Y. Kitagawa, T. Takahashi, T. Ikeda, Y. Honda, and S. Okuda, Rev. Sci. Instrum. **76** (2005), 10.1063/1.1824371.

[26]S. Masuda, E. Miura, K. Koyama, and S. Kato, Rev. Sci. Instrum. **79**, 083301 (2008).

[27]K. Zeil, S. D. Kraft, A. Jochmann, F. Kroll, W. Jahr, U. Schramm, L. Karsch, J. Pawelke, B. Hidding, and G. Pretzler, Rev. Sci. Instrum. **81**, 013307 (2010).

[28]T. Bonnet, M. Comet, D. Denis-Petit, F. Gobet, F. Hannachi, M. Tarisien, M. Versteegen, and M. M. Aleonard, Rev. Sci. Instrum. **84** (2013), 10.1063/1.4775719.

[29]A. Buck, K. Zeil, A. Popp, K. Schmid, A. Jochmann, S. D. Kraft, B. Hidding, T. Kudyakov, C. M. S. Sears, L. Veisz, S. Karsch, J. Pawelke, R. Sauerbrey, T. Cowan, F. Krausz, and U. Schramm, Rev. Sci. Instrum. **81**, 033301 (2010).

[30]R. Morlotti, M. Nikl, M. Piazza, and C. Boragno, J. Lumin. **72-74**, 772 (1997).

[31]B. Hidding, G. Pretzler, M. Clever, F. Brandl, F. Zamponi, A. Lübcke, T. Kämpfer, I. Uschmann, E. Förster, U. Schramm, R. Sauerbrey, E. Kroupp, L. Veisz, K. Schmid, S. Benavides, and S. Karsch, Rev. Sci. Instrum. **78**, 083301 (2007).

[32]Y. Glinec, J. Faure, A. Guemnie-Tafo, V. M. Monard, J. P. Larbre, V. De Waele, J. L. Marignier, M. Mostafavi, V. Malka, and H. Monard, Rev. Sci. Instrum. **77**, 103301 (2006).

[33]K. Nakamura, A. J. Gonsalves, C. Lin, A. Smith, D. Rodgers, R. Donahue, W. Byrne, and W. P. Leemans, Phys. Rev. Accel. Beams **14**, 062801 (2011).

[34]G. E. Giakoumakis and D. M. Miliotis, Phys. Med. Biol. **30**, 21 (1985).